Large Q^2 electrodisintegration of the deuteron in the virtual nucleon approximation

Misak M. Sargsian
Florida International University, Miami, Florida 33199, USA
(Received 8 December 2009; published 26 July 2010)

The two-body breakup of the deuteron is studied at high-Q^2 kinematics, with the main motivation to probe the deuteron at small internucleon distances. Such studies are associated with the probing of the high-momentum component of the deuteron wave function. For this, two main theoretical issues have been addressed: electromagnetic interaction of the virtual photon with the bound nucleon and the strong interaction of produced baryons in the final state of the breakup reaction. Within virtual nucleon approximation we developed a new prescription to account for the bound nucleon effects in electromagnetic interaction. The final-state interaction at high-Q^2 kinematics is calculated within the generalized eikonal approximation (GEA). We studied the uncertainties involved in the calculation and performed comparisons with the first experimental data on deuteron electrodisintegration at large Q^2. We demonstrate that the experimental data confirm the GEA's early prediction that the rescattering is maximal at $\sim 70^\circ$ of recoil nucleon production relative to the momentum of the virtual photon. Comparisons also show that the forward recoil nucleon angles are best suited for studies of the electromagnetic interaction of bound nucleons and the high-momentum structure of the deuteron. Backward recoil angle kinematics show sizable effects owing to the Δ-isobar contribution. The latter indicates the importance of further development of the GEA to account for the inelastic transitions in the intermediate state of the electrodisintegration reactions.

DOI: 10.1103/PhysRevC.82.014612 PACS number(s): 25.10.+s, 11.80.Fv, 25.30.Fj, 25.30.Rw

I. INTRODUCTION

Two-body electrodisintegration of the deuteron at high Q^2 represents a powerful tool for studying one of the most fundamental issues of nuclear physics: nuclear forces at intermediate to short distances. Despite all the successes in constructing interaction potentials for NN scattering, the most advanced potentials [1–4] still use phenomenological form factors to account for intermediate- to short-range interactions. Such form factors shed little light on how nuclear forces at short distances follow from the basic concepts of QCD. Presently, only the long-range NN interaction is understood on fundamental QCD grounds.

The situation is not spectacular also from the experimental point of view. New experiments aimed at studies of NN interaction at short distances practically stopped after the reassignment of AGS at Brookhaven National Laboratory.[1]

In this respect, an alternative way of studying nuclear forces at short distances is to probe NN systems in nuclei at short space-time separations. Expectations that this can be achieved only at high-momentum transfer reactions (see, e.g., Refs. [7–11]) were confirmed in a series of experiments with high-energy electron [12–16] and proton probes [17–21]. Some of the unique results of these experiments were the observations of the scaling for the ratios of inclusive cross sections of nuclei and the deuteron [12] (or ^{3}He [13,14]) at $x_{Bj} > 1$ at $Q^2 > 1.5$ GeV^2, as well as the observation of the strong (by factor of 20) dominance of pn relative to pp/nn short-range correlations in the ^{12}C nucleus for bound nucleon momenta 300–600 MeV/c [15,16,21]. If the first result was an indication that two (or more) nucleons can be probed at small separations, the second one was an indication of the dominance of the tensor forces [22–24] in such correlations.

The simplest reaction which could be used to investigate short-range NN interactions using nuclear targets is the exclusive electrodisintegration of the deuteron in which large magnitudes of the relative momentum of the pn system in the ground state are probed. Three experiments [25–27] have already been performed using the relatively high (up to 6 GeV)-energy electron beam of the Jefferson Lab and a more comprehensive experimental program will follow after the 11-GeV upgrade of the laboratory [28].

The prospect of having detailed experimental data on high-energy deuteron electrodisintegration makes the development of theoretical approaches for description of these reactions a pressing issue.

One of the first models for high-energy breakup of the deuteron were developed in the mid-1990s, in which the main emphasis was given to the studies of nucleon rescattering in the final state of the reactions [29–32]. These models were simple in a way that they assumed a factorization of the electromagnetic $\gamma^* N$ and final-state NN interactions and considered the rather small values of relative momenta of the bound pn system.

The extension of these calculations to a larger internal momentum region required more elaborate approaches, and several studies were done in this direction [10,33–39].

In this work we develop a theoretical model for the description of high-Q^2 exclusive electrodisintegration of the deuteron in knockout kinematics based on virtual nucleon approximation. The main theoretical framework is based on the generalized eikonal approximation (GEA) [10,31,35,40–43], which allows us to represent the scattering amplitude in the covariant form using effective Feynman diagram rules. In this

[1]The best hopes for the restart of the program of high-energy baryonic experiments are associated with the upcoming projects of J-PARC, Japan [5], and GSI, Germany [6].

way all the virtualities involved in the scattering amplitudes are defined unambiguously. Reducing these amplitudes by choosing positive energy projections for the nucleon propagators allows us to represent them through the convolutions of the deuteron wave function, on- and off-shell components of electromagnetic current, and pn rescattering amplitude. In addition to accounting for the off-shell effects, nonfactorized approximation is applied to the electromagnetic and NN rescattering parts in the calculation of the final-state interaction (FSI) amplitude. As a result, our calculation extends beyond the distorted wave impulse approximation limit. We also estimated the charge-exchange contribution in the FSI in addition to the $pn \to pn$ rescattering part of the FSI amplitude included in the eikonal approximation.

The article is organized as follows. In Sec. II we briefly discuss the kinematics of the disintegration reaction which we consider most efficient in probing the pn system at small separations. Then we discuss the basic assumptions of virtual nuclear approximation and proceed with the derivation of scattering amplitudes and the differential cross section of the reaction.

In Sec. III, after deriving the total scattering amplitude, we perform a detailed theoretical analysis to identify the extent of uncertainties owing to the off-shell part of the FSI, as well as contribution owing to charge-exchange rescattering. We also analyzed the role of the off-shell effects in the electromagnetic current of the bound nucleon. These analyses allowed us to conclude that at sufficiently large values of Q^2 ($\sim$6 GeV^2) the three most important contributions into the disintegration process are the off-shell electromagnetic current of the bound nucleon, the deuteron wave function, and the on-shell part of the NN scattering amplitude.

Furthermore, we compare our calculations with the first available high-Q^2 experimental data. These comparisons allow us to confirm the early prediction of the GEA that the maximal strength of FSI corresponds to $\sim 70^\circ$ production of the recoil nucleon relative to the direction of the virtual photon. We also found that forward angles of recoil nucleon are best suited for studies of the off-shell electromagnetic current and the deuteron wave function. Another observation is that in the backward direction there is a sizable contribution owing to the Δ-isobar production at the intermediate state of the reaction. In Sec. IV we give conclusions and an outlook on further development of the model.

II. CROSS SECTION OF THE REACTION

A. Kinematics

We discuss the process

$$e + d \to e' + p + n \tag{1}$$

in knockout kinematics in which case one nucleon (for definiteness we consider it to be a proton) absorbs the virtual photon and carries almost all of its momentum. The optimal kinematics for probing the initial pn system at close distances is defined as follows:

$$\begin{aligned} &\text{(a) } Q^2 \geqslant 1 \text{ GeV}^2; \quad \text{(b) } \vec{p}_f \approx \vec{q}; \\ &\text{(c) } p_f \gg p_r \geqslant 300 \text{ MeV}/c, \end{aligned} \tag{2}$$

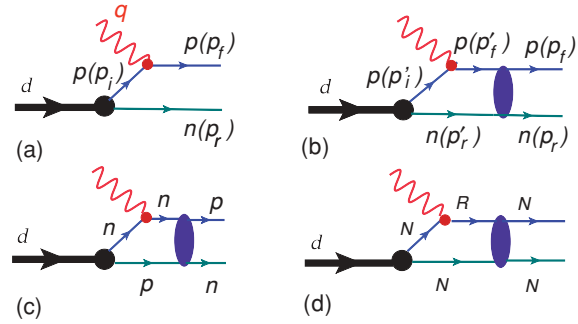

FIG. 1. (Color online) GEA diagrams.

where we define $q \equiv (q_0, \vec{q})$, $p_f \equiv (E_f, \vec{p}_f)$, and $p_r = (E_r, \vec{p}_r)$ as four-momenta of virtual photon, knockout proton, and recoil neutron, respectively. Also, $Q^2 = |\vec{q}|^2 - q_0^2$. Conditions (2)(b) and (2)(c) define the knockout process, while condition (2)(a) is necessary to satisfy Eq. (2)(c). From the point of view of the dynamics of the reaction, one also needs Eq. (2)(a) to provide a necessary resolution for probing the deuteron at small internucleon distances.

In the most simple picture the kinematics of Eq. (2) represent a scenario in which the high-energy virtual photon removes the proton from the pn system, leaving the neutron with the pre-existing relative momentum p_r [see Fig. 1(a)].

B. Main assumptions of virtual nucleon approximation

The virtual nucleon approximation is based on the following main assumptions, which also define the limits of its validity. First, one considers only the pn component of the deuteron, neglecting inelastic initial-state transitions. Because the deuteron is in a isosinglet state, this will correspond to restricting the kinetic energy of recoil nucleon to

$$T_N < 2(m_\Delta - m_N) \sim (m_{N^*} - m) \sim 500 \text{ MeV}, \tag{3}$$

where m, m_Δ, and m_{N^*} are masses of the nucleon and low-lying nonstrange baryonic resonances $\Delta(1232)$ and $N^*(1525)$. We neglect also the pionic degrees of freedom in the deuteron wave function. However, we expect that the overall error introduced by this approximation to be small because the probability of low-momentum pionic degrees of freedom is suppressed owing to the pseudo-Goldstone nature of pions in QCD, as well as the observation that πNN form factors are soft (see, e.g., discussion in Refs. [8,11]).

The second assumption is that the negative energy projection of the virtual nucleon propagator gives negligible contribution to the scattering amplitude. Such an assumption can be justified if

$$M_d - \sqrt{m^2 + p^2} > 0, \tag{4}$$

where M_d is the mass of the deuteron and p is the relative momentum of the bound pn system.

The preceding two conditions can be satisfied if we restrict the momentum of the recoil neutron, $p_r \leqslant 700$ MeV/c. However, owing to the fact that we explicitly left out the non-nucleonic components of deuteron wave function, the

momentum sum rule is not satisfied in virtual nucleon approximation (see discussions in Refs. [8,44,45]).

The third assumption that is made in the calculations is that at large Q^2 (>1 GeV^2) the interaction of virtual photon with exchanged mesons are a small correction and can be neglected (see, e.g., discussions in Refs. [9,10]).

C. Generalized eikonal approximation

The previously discussed assumptions allow us to restrict the consideration by the set of Feynman diagrams presented in Fig. 1. One can calculate these diagrams based on the effective Feynman diagram rules discussed in Ref. [10]. These rules allow us to formulate scattering amplitudes in the covariant form which unambiguously accounts for all the off-shell effects. Then we reduce the covariant amplitudes into a noncovariant form by choosing the positive energy projection of nucleon (or baryonic resonance) propagators at the intermediate state of the reaction.

The diagram in Fig. 1(a) corresponds to the plane wave impulse approximation (PWIA), in which the virtual photon knocks out one of the nucleons from the deuteron, leaving the second nucleon in the on-shell positive energy state. Two nucleons do not interact in the final state of the reaction, representing two outgoing plane waves. The diagram in Fig. 1(b) represents a situation in which the elastic electroproduction is followed by the elastic $pn \to pn$ rescattering. In this case, the rescattering is forward in the sense that, for example, the proton struck by the virtual photon will attain its large momentum after the $pn \to pn$ rescattering. The amplitude of this scattering will be referred to as a forward FSI amplitude.

The diagram of Fig. 1(c) corresponds to the scenario in which FSI proceeds through the charge-exchange $pn \to np$ rescattering. In this case the final fast proton emerges from the process in which the photon strikes the neutron, which then undergoes a $np \to pn$ charge-exchange rescattering. The amplitude of this scattering process will be referred to as a charge-exchange FSI amplitude.

The fourth diagram [Fig. 1(d)] corresponds to the electroproduction of an excited state R with a subsequent $RN \to NN$ final-state rescattering. The most important contribution to the fourth diagram is attributable to the Δ-isobar (IC), whose production threshold is closest to the quasielastic scattering kinematics. Several factors make IC contribution small in the high-Q^2 limit at $x \geqslant 1$ [9,10]. One factor is the large longitudinal momenta of the initial nucleon involved in the Δ-electroproduction process,

$$p_{i,z}^{IC} = (1-x)m - \frac{m_\Delta^2 - m^2}{2q}, \tag{5}$$

which indicates that choosing $x > 1$ one can suppress the electroproduction of Δ resonance in the intermediate states owing to the large values of initial momenta entering in the deuteron wave function.

An additional suppression of IC follows from the smallness of the $\gamma^* N \to \Delta$ transition form factors, as compared to the elastic form factors at $Q^2 \geqslant$ few GeV^2 [46,47]. Finally, owing to the fact that the $\Delta N \to NN$ amplitude is dominated by pion or ρ-type reggeon exchanges, it will be additionally suppressed by at least the factor of $\frac{1}{\sqrt{Q^2}}$. In any case, this contribution can be calculated in a self-consistent way within the GEA. The calculation of these types of diagrams within the GEA will be presented elsewhere [48].

In what follows we discuss the calculations of only the first three diagrams of Fig. 1.

1. Plane wave impulse approximation amplitude

The amplitude of the PWIA diagram in the covariant form can be written as follows:

$$\langle s_f, s_r | A_0^\mu | s_d \rangle = -\bar{u}(p_r, s_r)\bar{u}(p_f, s_f)\Gamma^\mu_{\gamma^* p} \times \frac{\not{p}_i + m}{p_i^2 - m^2} \cdot \Gamma_{DNN} \cdot \chi^{s_d}, \tag{6}$$

where $\Gamma_{\gamma^* p}$ is the electromagnetic vertex of the $\gamma^* N \to N$ scattering and the vertex function Γ_{DNN} describes the transition of the deuteron into the pn system. The notations s_d, s_f, and s_r describe the spin projections of the deuteron, knockout proton, and recoil neutron, respectively. The spin function of the deuteron is represented by χ^{s_d}. The four-momentum of the struck nucleon in the initial state within PWIA is defined as

$$p_i = (E_d - E_r, \vec{p}_d - \vec{p}_r) = (M_d - E_r, -\vec{p}_r)|_{LaB}. \tag{7}$$

The preceding relation clearly shows the off-shell character of the struck nucleon in the initial state, because $p_i^2 \neq m^2$. Therefore, expressing the initial nucleon's propagator through the on-mass shell nucleonic spinors is not valid.

However, using an approximation in which only positive energy projections are taken into account, one can isolate the on-shell part of the propagator by adding and subtracting $E_i^{\text{on}}\gamma^0$ term to $\not{p}_i$ as follows:

$$\not{p}_i + m = \not{p}_i^{\text{on}} + m + \left(E_i^{\text{off}} - E_i^{\text{on}}\right)\gamma^0, \tag{8}$$

where $E_i^{\text{off}} = M_d - \sqrt{m_n^2 + p_r^2}$ and $E_i^{\text{on}} = \sqrt{m_p + p_r^2}$, where m_n and m_p are the masses of the proton and neutron, respectively.[2] Now we can separate the PWIA amplitude into on- and off-shell parts in the following way:

$$\langle s_f, s_r | A_0^\mu | s_d \rangle = \langle s_f, s_r | A_{0,\text{on}}^\mu | s_d \rangle + \langle s_f, s_r | A_{0,\text{off}}^\mu | s_d \rangle, \tag{9}$$

where

$$\langle s_f, s_r | A_{0,\text{on}}^\mu | s_d \rangle = -\bar{u}(p_f, s_f)\Gamma^\mu_{\gamma^* p} \frac{\not{p}_i^{\text{on}} + m}{p_i^2 - m^2} \cdot \bar{u}(p_r, s_r)\Gamma_{DNN}\chi_d^s, \tag{10}$$

and

$$\langle s_f, s_r | A_{0,\text{off}}^\mu | s_d \rangle = -\bar{u}(p_f, s_f)\Gamma^\mu_{\gamma^* p} \frac{\left(E_i^{\text{off}} - E_i^{\text{on}}\right)\gamma^0}{p_i^2 - m^2} \cdot \bar{u}(p_r, s_r)\Gamma_{DNN}\chi_d^s. \tag{11}$$

[2] In further discussion, we neglect the difference between proton and neutron masses, denoting them by m.

For the on-shell part of the amplitude, using

$$\not{p}_i^{\rm on} + m = \sum_{s_i} u(p_i, s_i)\bar{u}(p_i, s_i) \tag{12}$$

and the definition [49,50]

$$\Psi_d^{s_d}(s_1, p_1, s_2, p_2) = -\frac{\bar{u}(p_1, s_1)\bar{u}(p_2, s_2)\Gamma^{s_d}_{DNN}\chi_{s_d}}{\left(p_1^2 - m^2\right)\sqrt{2}\sqrt{(2\pi)^3 2\left(p_2^2 + m^2\right)}^{\frac{1}{2}}}, \tag{13}$$

one obtains

$$\langle s_f, s_r|A^\mu_{0,\rm on}|s_d\rangle = \sqrt{2}\sqrt{(2\pi)^3 2E_r}\sum_{s_i} J^\mu_{N,\rm on}(s_f, p_f; s_i, p_i) \times \Psi_d^{s_d}(s_i, p_i, s_r, p_r), \tag{14}$$

where

$$J^\mu_{N,\rm on}(s_f, p_f; s_i, p_i) = \bar{u}(p_f, s_f)\Gamma^\mu_{\gamma^* N} u(p_i, s_i). \tag{15}$$

For the off-shell part of the scattering amplitude, one observes that the relation

$$\bar{u}(p_2, s_2)\Gamma_{DNN}\chi^{s_d} = -\sum_{s_1}\frac{u(p_1, s_1)\Psi_d^{s_d}(s_1, p_1, s_2, p_2)}{2m} \times \left(p_1^2 - m^2\right)\sqrt{2}\sqrt{(2\pi)^3 2\left(p_2^2 + m^2\right)}^{\frac{1}{2}} \tag{16}$$

satisfies Eq. (13). Inserting it into Eq. (11), one obtains

$$\langle s_f, s_r|A^\mu_{0,\rm off}|s_d\rangle = \sqrt{2}\sqrt{(2\pi)^3 2E_r}\sum_{s_i} J^\mu_{N,\rm off}(s_f, p_f; s_i, p_i) \times \Psi_d^{s_d}(s_i, p_i, s_r, p_r), \tag{17}$$

where

$$J^\mu_{N,\rm off}(s_f, p_f; s_i, p_i) = \bar{u}(p_f, s_f)\Gamma^\mu_{\gamma^* N}\gamma^0 u(p_i, s_i)\frac{E_i^{\rm off} - E_i^{\rm on}}{2m}, \tag{18}$$

and $E_i^{\rm off} = M_d - E_i^{\rm on}$ and $E_i^{\rm on} = \sqrt{m^2 + p_i^2}$.

One can combine on- and off-shell parts of the PWIA scattering amplitudes in the following form:

$$\langle s_f, s_r|A^\mu_0|s_d\rangle = \sqrt{2}\sqrt{(2\pi)^3 2E_r}\sum_{s_i} J^\mu_N(s_f, p_f; s_i, p_i) \times \Psi_d^{s_d}(s_i, p_i, s_r, p_r), \tag{19}$$

where

$$J^\mu_N(s_f, p_f; s_i, p_i) = J^\mu_{N,\rm on}(s_f, p_f; s_i, p_i) + J^\mu_{N,\rm off}(s_f, p_f; s_i, p_i). \tag{20}$$

The preceding form of the electromagnetic current, together with Eqs. (15) and (18), represents our off-shell approximation. It is worth noting that the first, "on-shell" part of this current corresponds to the widely used "De Forest" approximation [51]. In the DeForest approximation because of the absence of the second term the gauge invariance is violated and the current conservation is restored by expressing J_0 or J_z components through each other with different assumptions for the nucleon spinors and electromagnetic vertices. The latter introduces more uncertainty because imposed relations are not unique. As a result, one generates several forms of the off-shell electromagnetic currents [51].

The additional "off-shell" part of the electromagnetic current in Eq. (20) obtained in our approximation reduces the uncertainty of choosing on-shell nucleon spinors which is inherent to the De Forest approximation. The total current in Eq. (20) is conserved because it is derived from the gauge invariant amplitude of Eq. (6). Therefore, our approximation does not violate gauge invariance and no additional conditions are needed to restore the current conservation.

Note that our approximation is analogous to the one used in hadronic physics within light-cone approximation (see, e.g., [52]), in which case an off-shell "γ^+" component of the fermion propagator is isolated in a manner similar to that done for the γ^0 component in our case.

2. *Forward elastic final-state interaction amplitude*

We start by applying effective Feynman diagram rules to the diagram of Fig. 1(b), which yields

$$\langle s_f, s_r|A^\mu_1|s_d\rangle = -\int\frac{d^4 p'_r}{i(2\pi)^4}\frac{\bar{u}(p_f, s_f)\bar{u}(p_r, s_r)F_{NN}[\not{p}'_r + m][\not{p}_d - \not{p}'_r + \not{q} + m]}{(p_d - p'_r + q)^2 - m^2 + i\epsilon} \times\frac{\Gamma^\mu_{\gamma^* N}[\not{p}_d - \not{p}'_r + m]\Gamma_{DNN}\chi^{s_d}}{[(p_d - p'_r)^2 - m^2 + i\epsilon]\left(p'^2_r - m^2 + i\epsilon\right)}, \tag{21}$$

were F_{NN} represents the invariant $pn \to pn$ scattering amplitude that can be expressed as follows:

$$F_{NN}(s, t) = \sqrt{s(s - 4m^2)}f_{NN}(s, t), \tag{22}$$

where s is the total invariant energy of the scattering pn system and the f_{NN} scattering amplitude is defined in such a way that $\mathrm{Im}\, f_{NN} = \sigma_{\rm tot}$. Furthermore, we use the following four-vectors defined as

$$p'_i = p_d - p'_r \quad \text{and} \quad p'_f = p_d - p'_r + q. \tag{23}$$

We first integrate by $d^0 p'_r$ through the positive energy pole of the spectator nucleon propagator at the intermediate state:

$$\int\frac{d^0 p'_r}{p'^2_r - m^2 + i\epsilon} = -i\frac{2\pi}{2E'_r}. \tag{24}$$

This integration allows us to use $\not{p}'_r + m = \sum_{s'_r} u(p'_r, s'_r)\bar{u}(p'_r, s'_r)$. For $\not{p}_d - \not{p}'_r$ we use a relation similar to Eq. (8). The same could be done for $\not{p}_d - \not{p}'_r + \not{q}$. However, for large values of q the off-shell part in Eq. (8) is suppressed by $\frac{|\vec{q}|-q_0}{|\vec{q}|}$ and in the large-Q^2 limit its contribution is negligible. Thus, we can use the on-shell relation, $\not{p}_d - \not{p}' + \not{q} + m = \sum_{s'_f} u(p'_f, s'_f)\bar{u}(p'_f, s'_f)$ for the knockout nucleon spinors in the intermediate state. Using the preceding representations of the spinors, the definitions of the deuteron wave function [Eq. (13)], and electromagnetic current [Eq. (20)] for the scattering amplitude of Eq. (21), we obtain

$$\begin{aligned}\langle s_f, s_r|A_1^\mu|s_d\rangle = -\sqrt{2}(2\pi)^{\frac{3}{2}} \sum_{s'_f,s'_r,s_i} \\ \times \int \frac{d^3p'_r}{(2\pi)^3} \frac{\sqrt{2E'_r}\sqrt{s(s-4m^2)}}{2E'_r[(p_d - p'_r + q)^2 - m^2 + i\epsilon]} \\ \times \langle p_f, s_f; p_r, s_r|f^{NN}(t,s)|p'_r, s'_r; p'_f, s'_f\rangle \\ \cdot J_N^\mu(s'_f, p'_f; s_i, p'_i) \cdot \Psi_d^{s_d}(s_i, p'_i, s'_r, p'_r).\end{aligned} \tag{25}$$

Next, we consider the propagator of the knockout proton in the intermediate state, using the condition of quasielastic scattering

$$(q + p_d - p_r)^2 = p_f^2 = m^2, \tag{26}$$

one obtains

$$(p_d - p'_r + q)^2 - m^2 + i\epsilon = 2|\mathbf{q}|(p'_{r,z} - p_{r,z} + \Delta + i\epsilon), \tag{27}$$

where

$$\Delta = \frac{q_0}{|\mathbf{q}|}(E_r - E'_r) + \frac{M_d}{|\mathbf{q}|}(E_r - E'_r). \tag{28}$$

Furthermore, using the relation

$$\begin{aligned}\frac{1}{p'_{r,z} - p_{r,z} + \Delta + i\epsilon} = -i\pi\delta[p'_{r,z} - (p_{r,z} - \Delta)] \\ + \mathcal{P}\int \frac{1}{p'_{r,z} - (p_{r,z} - \Delta)}\end{aligned} \tag{29}$$

and performing integration over $p'_{r,z}$, we split the scattering amplitude into two terms, one containing on-shell and the other off-shell $pn \to pn$ scattering amplitudes as follows:

$$\begin{aligned}&\langle s_f, s_r|A_1^\mu|s_d\rangle \\ &= \frac{i\sqrt{2}(2\pi)^{\frac{3}{2}}}{4} \sum_{s'_f,s'_r,s_i} \int \frac{d^2p'_r}{(2\pi)^2} \frac{\sqrt{2\tilde{E}'_r}\sqrt{s(s-4m^2)}}{2\tilde{E}'_r|q|} \\ &\times \langle p_f, s_f; p_r, s_r|f^{NN,\mathrm{on}}(t,s)|\tilde{p}'_r, s'_r; \tilde{p}'_f, s'_f\rangle \\ &\cdot J_N^\mu(s'_f, p'_f; s_i, \tilde{p}'_i) \cdot \Psi_d^{s_d}(s_i, \tilde{p}'_i, s'_r, \tilde{p}'_r) \\ &- \frac{\sqrt{2}(2\pi)^{\frac{3}{2}}}{2} \sum_{s'_f,s'_r,s_i} \mathcal{P}\int \frac{dp'_{r,z}}{2\pi} \int \frac{d^2p'_r}{(2\pi)^2} \\ &\times \frac{\sqrt{2E'_r}\sqrt{s(s-4m^2)}}{2E'_r|\mathbf{q}|} \\ &\times \frac{\langle p_f, s_f; p_r, s_r|f^{NN,\mathrm{off}}(t,s)|p'_r, s'_r; p'_f, s'_f\rangle}{p'_{r,z} - \tilde{p}'_{r,z}} \\ &\times J_N^\mu(s'_f, p'_f; s_i, p'_i) \cdot \Psi_d^{s_d}(s_i, p'_i, s'_r, p'_r),\end{aligned} \tag{30}$$

where $\tilde{p}'_r = (p_{r,z} - \Delta, p'_{r,\perp})$, $\tilde{E}'_r = \sqrt{m^2 + \tilde{p}'^2_r}$, $\tilde{p}'_i = p_d - \tilde{p}'_r$, and $\tilde{p}'_f = \tilde{p}'_i + q$.

For numerical estimates of the preceding amplitudes, one needs on- and off-shell $pn \to pn$ amplitudes as an input. In the high-energy limit in which the helicity conservation of small-angle NN scattering is rather well established, the on-shell amplitude is predominantly imaginary and can be parameterized in the form

$$\begin{aligned}&\langle p_f, s_f; p_r, s_r|f^{NN,\mathrm{on}}(t,s)|\tilde{p}'_r, s'_r; \tilde{p}'_f, s'_f\rangle \\ &= \sigma_{\mathrm{tot}}^{pn}(i+\alpha)e^{\frac{B}{2}t}\delta_{s_f,s'_f}\delta_{s_r,s'_r},\end{aligned} \tag{31}$$

where $\sigma_{\mathrm{tot}}^{pn}(s)$, $B(s)$, and $\alpha(s)$ are found from fitting of experimental data on elastic $pn \to pn$ scattering. For the effective laboratory momentum range of up to 1.3 GeV/c, the SAID parametrization [53] of pn amplitudes can be used. In our numerical estimates, the SAID parametrization is implemented, similar to Ref. [37], by expressing them through the Saclay (a, b, c, d, and e [54]) amplitudes (see also the discussion for the parametrization of the charge-exchange amplitude in Sec. II C3). We used cubic spline to interpolate between the central (spin-conserving) part of the SAID amplitudes (at $t = 0$) and the amplitude parameterized in the diffractive form at laboratory momenta $\geqslant 2$ GeV/c. In the same way we interpolated the slope factor and the real part of the central amplitude. For the spin-flip part we extrapolated the SAID amplitudes to the $\geqslant 1.3$ GeV/c region assuming that their magnitudes decrease with the invariant energy as $\frac{1}{\sqrt{s_{NN}}}$. The latter corresponds to the assumption that the spin-flip amplitudes are attributable to the pion exchange.[3]

The situation is more uncertain for the half-off-shell part of the $f^{NN,\mathrm{off}}$ amplitude. In the present calculations we use the following parametrization:

$$f^{NN,\mathrm{off}} = f^{NN,\mathrm{on}} e^{B(m_{\mathrm{off}}^2 - m^2)}, \tag{32}$$

where $m_{\mathrm{off}}^2 = (M_d - E'_r + q_0)^2 - (p'_r + q)^2$. Overall, we expect that our calculation will not be reliable in situations in which the contribution from the off-shell part of the rescattering is dominant. However, in the high-Q^2 limit this contribution is only a small correction.

Completing this section it is worth noticing that in addition to the appearance of the Δ factor [Eq. (28)] in the GEA which does not enter in conventional Glauber approximation (see detailed discussion in Ref. [10]), the new factor, $\frac{\sqrt{s(s-4m^2)}}{2E'_r|q|}$ entering the elastic FSI amplitude [Eq. (30)] is also unique to the GEA. Within conventional Glauber approximation, in

[3]Note, however, that in the $Q^2 > 1$ GeV^2 region the contribution of spin-flip FSI effects in the unpolarized cross section is a small correction.

which Fermi motion of the scatterers is neglected, this factor is equal to one. However, within the GEA it appears as a consequence of the covariant form of the initial scattering amplitude. Calculation of this factor for our kinematics yields

$$\frac{\sqrt{s(s-4m^2)}}{2E'_r|q|} = \frac{\sqrt{\left(\frac{2-x}{x}Q^2+m_D^2\right)\left(\frac{2-x}{x}Q^2\right)}}{2E'_r|q|}, \qquad (33)$$

which decreases with $x \to 2$. Thus, for the $x > 1$ and large-Q^2 kinematics, the GEA predicts an additional suppression of FSI as compared to the conventional Glauber approximation.

3. Charge-exchange final-state interaction amplitude

To complete the calculation of the total amplitude, we need to include the contribution from charge-exchange rescattering, which can be obtained from Eq. (30) after the substitutions corresponding to Fig. 1(c). Namely, one needs to switch the proton and neutron lines in the initial and intermediate states of the scattering, replace proton electromagnetic current with the neutron and f_{NN} with the charge-exchange scattering amplitude $f_{NN}^{\rm chex}$. One obtains

$$\begin{aligned}
&\langle s_f, s_r|A^{\mu}_{1,\rm chex}|s_d\rangle \\
&= \frac{i\sqrt{2}(2\pi)^{\frac{3}{2}}}{4}\sum_{s'_f,s'_r,s_i}\int\frac{d^2p'_r}{(2\pi)^2}\frac{\sqrt{2\tilde{E}'_r}\sqrt{s(s-4m^2)}}{2\tilde{E}'_r|q|} \\
&\times\langle p_f, s_f; p_r, s_r|f^{\rm chex,on}(t,s)|\tilde{p}'_r, s'_r; \tilde{p}'_f, s'_f\rangle \\
&\cdot J^{\mu}_n(s'_f, p'_f; s_i, \tilde{p}'_i)\cdot\Psi^{s_d}_d(s_i, \tilde{p}'_i, s'_r, \tilde{p}'_r) \\
&-\frac{\sqrt{2}(2\pi)^{\frac{3}{2}}}{2}\sum_{s'_f,s'_r,s_1}\mathcal{P}\int\frac{dp'_{r,z}}{2\pi}\int\frac{d^2p'_r}{(2\pi)^2} \\
&\times\frac{\sqrt{2E'_r}\sqrt{s(s-4m^2)}}{2E'_r|\mathbf{q}|} \\
&\times\frac{\langle p_f, s_f; p_r, s_r|f^{\rm chex,off}(t,s)|p'_r, s'_r; p'_f, s'_f\rangle}{p'_{r,z}-\tilde{p}'_{r,z}} \\
&\times J^{\mu}_n(s'_f, p'_f; s_i, p'_i)\cdot\Psi^{s_d}_d(s_i, p'_i, s'_r, p'_r). \qquad (34)
\end{aligned}$$

Here the charge-exchange rescattering amplitude $f_{NN}^{\rm chex}$, similar to the elastic FSI case, is taken from the experimental measurements. The off-shell extrapolation of the rescattering amplitude is also done similar to Eq. (32). For numerical estimates in the high-energy region we use the following parametrization of the Saclay amplitudes [55]:

$$\begin{aligned}
a &= \frac{N}{3}[g(p)+2g(q)], \\
b &= \frac{N}{3}[-g(p)-6f(q)g(q)+4g(q)], \\
c &= \frac{N}{3}[-3f(p)g(p)+2g(p)-2g(q)], \qquad (35)\\
d &= N[-f(p)g(p)+2f(q)g(q)], \\
e &= 0,
\end{aligned}$$

where $g(x) = (\frac{\Lambda^2}{x^2+\Lambda^2})^2$, $f(x) = \frac{x^2}{x^2+\mu^2}$, and $N = (\frac{m}{m_\pi})^2\frac{2}{\sqrt{s}}\frac{f_\pi^2}{4\pi}(\frac{\Lambda^2-\mu^2}{\Lambda^2})^2$, with $\Lambda = 748$ MeV, $\frac{f_\pi^2}{4\pi} = 0.079$, and $\mu = m_\pi = 140$ MeV. The transferred momenta are defined as $p^2 = -t$ and $q^2 = -u$. Note that the preceding defined amplitudes are real, which follows from the assumption that charge-exchange scattering is attributable to the pion exchange. These amplitudes are interpolated with the cubic Spline fit to the corresponding SAID amplitudes at lower energies.

4. Deuteron wave function

The deuteron wave function in Eq. (13) in general represents a solution of the Bethe-Salpeter-type equation. To fix the normalization of the wave function, we need to relate an expression that contains the deuteron wave function [as it is defined in Eq. (13)] to a well-defined quantity characterizing the deuteron. One such quantity is the deuteron elastic charge form factor G_C, which at $Q^2 \to 0$ limit approaches one; that is, $G_C(Q^2 = 0) = 1$ (see, e.g., Ref. [56]). The latter could be related to the deuteron elastic scattering amplitude as follows:

$$\frac{1}{4M_d}\sum_{s'_d=s_d=-1}^{1}\langle p'_d, s'_d|A^{\mu=0}(Q^2)|p_d, s_d\rangle|_{Q^2\to 0} = G_C(0) = 1, \qquad (36)$$

where $\langle p'_d, s'_d|A^{\mu}|p_d, s_d\rangle$ is the elastic $\gamma^* d \to d'$ scattering amplitude corresponding to the diagram of Fig. 2.

Applying the same effective Feynman diagram rules used earlier for $\langle p'_d, s'_d|A^{\mu}|p_d, s_d\rangle$, one obtains

$$\begin{aligned}
\langle p'_d, s'_d|A^{\mu}|p_d, s_d\rangle = -\sum_{p,n}\int\frac{d^4p_r}{i(2\pi)^4}\chi^{s'_d,\dagger}\Gamma^{\dagger}_{DNN} \\
\times\frac{\not{p}_2+m}{p_2^2-m^2+i\epsilon}\Gamma^{\mu}_{\gamma^*N}\frac{\not{p}_1+m}{p_1^2-m^2+i\epsilon} \\
\times\Gamma_{DNN}\chi^{s_d}\frac{\not{p}_r+m}{p_r^2-m^2+i\epsilon}. \qquad (37)
\end{aligned}$$

Further derivations within the virtual nucleon approximation follow steps similar to those seen in Secs. II C 1 and II C 2. We first evaluate dp_r^0 integral by the pole value of the spectator nucleon propagator, then separate the on- and off-shell parts in the numerator of interacting nucleon propagators and introduce deuteron wave function according to Eq. (13). In this case, the electromagnetic current of the nucleon is fully off-shell because the struck nucleon is bound in both initial and final states of the reaction. This results in the following expression

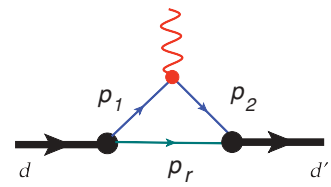

FIG. 2. (Color online) Elastic $\gamma^* d \to d'$ diagram.

for the elastic scattering amplitude:

$$\langle p'_d, s'_d|A^\mu|p_d, s_d\rangle = 4\sum_{p,n}\sum_{s_2,s_1,s_r}\int d^3p_r \Psi_d^{s'_d\dagger}(s_2, p_2, s_r, p_r) \times \bar{u}(p_2, s_2)\left[I + \frac{E_2^{\rm off} - E_2^{\rm on}}{2m}\gamma_0\right] \times \Gamma^\mu_{\gamma^* N}\left[I + \frac{E_1^{\rm off} - E_1^{\rm on}}{2m}\gamma_0\right] \times u(p_1, s_1)\Psi_d^{s_d}(s_1, p_1, s_r, p_r). \quad (38)$$

Neglecting the second-order off-shell terms in the preceding equation [i.e., $(\frac{E^{\rm off}-E^{\rm on}}{2m})^2$], one obtains

$$\langle p'_d, s'_d|A^\mu|p_d, s_d\rangle = 4\sum_{p,n}\sum_{s_2,s_1,s_r}\int d^3p_r \Psi_d^{s'_d\dagger}(s_2, p_2, s_r, p_r) \times \tilde{J}^\mu_N \Psi_d^{s_d}(s_1, p_1, s_r, p_r), \quad (39)$$

where

$$\tilde{J}^\mu_N(s_2, p_2; s_1, p_1) = J^\mu_{N,\rm on}(s_2, p_2; s_1, p_1) + J^\mu_{N,\rm off}\left(s_2, p_2^{\rm off}; s_1, p_1\right) + J^\mu_{N,\rm off}\left(s_2, p_2; s_1, p_1^{\rm off}\right). \quad (40)$$

Here the on- and off-shell parts of electromagnetic current are defined in Eqs. (15) and (18). In the preceding equation, the notation $p^{\rm off}$ in the argument of $J_{N,\rm off}$ indicates which nucleon is considered as off-shell.

Using now the fact that for the proton and neutron $F_{1p(n)}(Q^2 = 0) = 1(0)$ and using Eqs. (15) and (18), one obtains

$$\tilde{J}^{\mu=0}_p\big|_{Q^2\to 0} = 2E_1^{\rm off}, \quad \tilde{J}^{\mu=0}_n\big|_{Q^2\to 0} = 0. \quad (41)$$

Using these relations and inserting Eq. (39) into Eq. (36), one obtains

$$\sum_{s_d=-1}^{1}\int \left|\Psi_d^{s_d}(p)\right|^2 \frac{2E_{\rm off}}{M_d}d^3p = 1, \quad (42)$$

where $E^{\rm off} = M_d - \sqrt{m^2 + p^2}$. It is worth mentioning that the preceding normalization coincides with the normalization obtained from the baryon number conservation sum rule [44,45,57–61] for deep inelastic scattering off the deuteron,

$$\int |\Psi_d(\alpha, p_t)|^2 \alpha d^3p = 1, \quad (43)$$

where $\alpha = \frac{M_d - \sqrt{m^2+p^2} - p_z}{m}$ is the light-cone momentum fraction of the deuteron carried by the struck nucleon. As mentioned in Sec. II B, in virtual nucleon approximation owing to unaccounted non-nucleonic degrees of freedom, the wave function defined according to Eq. (13) will not satisfy the energy-momentum sum rule which expresses the requirement that the sum of the light-cone momentum fractions of all the constituents of the nucleus equals one.

For numerical estimates we model the deuteron wave function to satisfy Eq. (42) in the following form [45,59]:

$$\Psi_d(p) = \Psi_d^{\rm NR}(p)\frac{M_d}{2(M_d - \sqrt{m^2 + p^2})}, \quad (44)$$

which provides a smooth transition to the nonrelativistic wave function $\Psi^{\rm NR}$ in the small momentum limit.

5. *Total amplitude and the differential cross section*

The total scattering amplitude consists of the sum of PWIA, forward, and charge-exchange FSI amplitudes:

$$\langle s_f, s_r|A^\mu|s_d\rangle = \langle s_f, s_r|A^\mu_0|s_d\rangle + \langle s_f, s_r|A^\mu_1|s_d\rangle + \langle s_f, s_r|A^\mu_{1,\rm chex}|s_d\rangle. \quad (45)$$

Using this amplitude, the differential cross section is calculated as follows:

$$\frac{d^5e\sigma}{dE'_e, d\Omega_{e'}d\Omega_f} = \frac{\alpha^2 E'_e}{q^4 E_e}\cdot\frac{1}{6}\sum_{s_f,s_r,s_d,s_1,s_2} \times \frac{\left|J^\mu_e J_{d,\mu}\right|^2}{2M_d E_f}\frac{p_f^2}{\left|\frac{p_f}{E_f} + \frac{p_f - q\cos(\theta_{pf,q})}{E_r}\right|}, \quad (46)$$

where

$$J^\mu_e = \bar{u}(k_2, s_2)\gamma^\mu u(k_1, s_1) \quad (47)$$

and

$$J^\mu_d = \frac{\langle s_f, s_r|A^\mu|s_d\rangle}{\sqrt{2(2\pi)^3 2E_r}}. \quad (48)$$

For numerical estimates we use the electromagnetic current of the nucleon in the form

$$\Gamma^\mu = F_1(Q^2)\gamma^\mu + \frac{F_2(Q^2)}{2m}i\sigma^{\mu,\nu}q_\nu, \quad (49)$$

where F_1 and F_2 are Dirac form factors and for their evaluation the available phenomenological parametrizations are used [62]. For the deuteron wave function we use the approximation of Eq. (44) with the nonrelativistic wave function calculated based on the Paris potential [4]. The pn scattering amplitude is parameterized in the form of Eq. (31) and its off-shell extrapolation in the form of Eq. (32). Also, for f_{pn} in the lower momentum range ($p_{\rm lab} \leqslant 1.3$ GeV/c) we use the SAID parametrization [53] based on the pn scattering phase shifts.

III. OBSERVABLES

The main quantity that we consider for numerical estimates is the ratio of the calculated cross section which includes total amplitude of Eq. (45) to the cross section calculated within PWIA:

$$R = \frac{\sigma}{\sigma^{\rm PWIA}}, \quad (50)$$

where $\sigma \equiv= \frac{d\sigma}{dE'_e, d\Omega_{e'}dp_f d\Omega_f}$. This ratio allows us to clearly distinguish between kinematics in which PWIA dominates $R \approx 1$ from kinematics in which FSI is dominated by screening $R < 1$ or single rescattering $R > 1$ effects (see, e.g., Refs. [31,40,63]).

Considering the numerical estimates of the ratio R, we discuss four main effects that characterize our present theoretical approach. These are the unfactorization of the electromagnetic interaction in the FSI amplitude, the off-shell effects in the FSI, the effects of charge-exchange rescatterings, and the off-shell effects in the electromagnetic interaction of the bound nucleon.

In our estimates we study the dependence of R on the angle of the recoil neutron relative to $\vec{q}$ for different values of neutron momenta. We perform our calculations for two values of Q^2 (2 and 6 GeV^2) which allows us to also assess the Q^2 dependence of the considered effects.

Finally, we present the comparisons with the first experimental data on the deuteron electrodisintegration at large Q^2.

A. Nonfactorization effects

In Fig. 3 we compare the calculations of R with and without factorization approximations for the electromagnetic current in the FSI amplitude. The factorization approximation will result in the so-called distorted wave impulse approximation (DWIA) widely used in the literature.

As the figure shows the factorization (or DWIA) approximation is applicable for up to $p_r \leqslant 300$ MeV/c or for the kinematics in which the FSI amplitude is smaller than the PWIA term. The factorization approximation breaks down in kinematics dominated by the rescattering process at $p_r \geqslant 400$ MeV/c. As the comparisons show, the unfactorization predicts a larger FSI amplitude which can be understood based on the fact that in this case the electromagnetic current which enters in the rescattering amplitude of Eq. (30) is defined at smaller values of bound nucleon momenta than the electromagnetic current in the PWIA term [Eq. (19)]. Our current results agree qualitatively with the previous analysis of nonfactorization effects presented in Ref. [33].

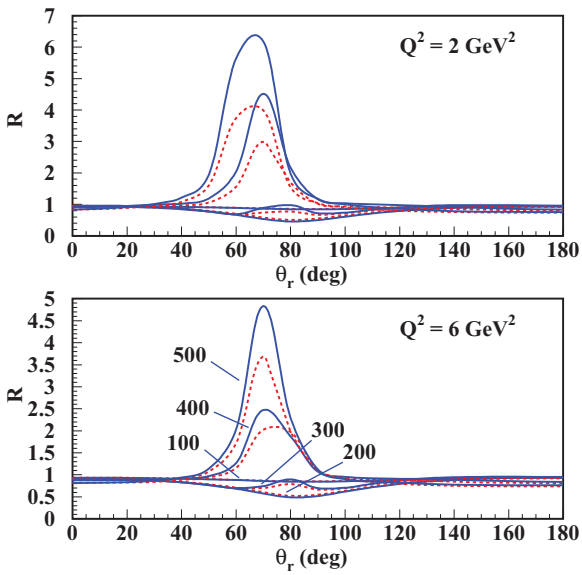

FIG. 3. (Color online) Dependence of ratio R on the recoil angle of the neutron for different values of $p_r = 100$, 200, 300, 400, 500 MeV/c and $Q^2 = 2$, 6 GeV^2. Solid line, unfactorized approximations; dashed line, factorized approximations.

Figure 3 shows also that the factorization approximation is Q^2-dependent and somewhat improves with an increase of Q^2. This is a rather important feature which should be taken into account in color transparency (CT) studies for double scattering kinematics, in which case the Q^2 dependence of the peak of the ratio R is studied to extract the CT signal (see, e.g., Refs. [31,63,64]). Our comparisons in Fig. 3 show that the unfactorized approximation should be used as a baseline for identification of the CT signature in the Q^2 dependence of the FSI contribution of the deuteron breakup cross section.

B. Off-shell FSI effects

Next we consider the contribution to the FSI amplitude owing to the principal value part of Eq. (30). This term depends on the half-off shell NN scattering amplitude, which is a largely unknown quantity. Therefore, the reliability of our calculations depends on the magnitude of the principal value term. In Fig. 4 we compare the calculations in which only the pole (on-shell) term of the FSI amplitude is included with the calculations which contain both pole (on-shell) and principal value (off-shell) terms of the FSI amplitude. For the half-off shell f_{pn} amplitude we use the approximation of Eq. (32). An important observation that can be made from Fig. 4 is that the off-shell rescattering effects diminish with an increase of Q^2. This is consistent with our earlier observation [11,12] that the distances that the virtual nucleon propagates before the rescattering decreases significantly with an increase of Q^2 at fixed values of x.

C. Charge-exchange rescattering effects

Owing to the fact that the charge-exchange rescattering amplitude is predominantly real, it will interfere mainly with

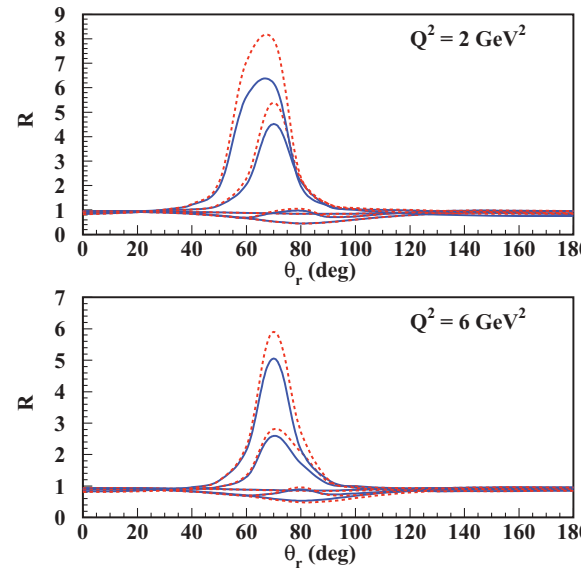

FIG. 4. (Color online) Dependence of ratio R on the recoil angle of the neutron for different values of p_r and $Q^2 = 2$, 6 GeV^2. The recoil neutron momenta are the same as in Fig. 3. Solid line, unfactorized calculation with the pole term only in the FSI amplitude; dashed line, unfactorized approximations with both pole and principal value terms in the FSI amplitude.

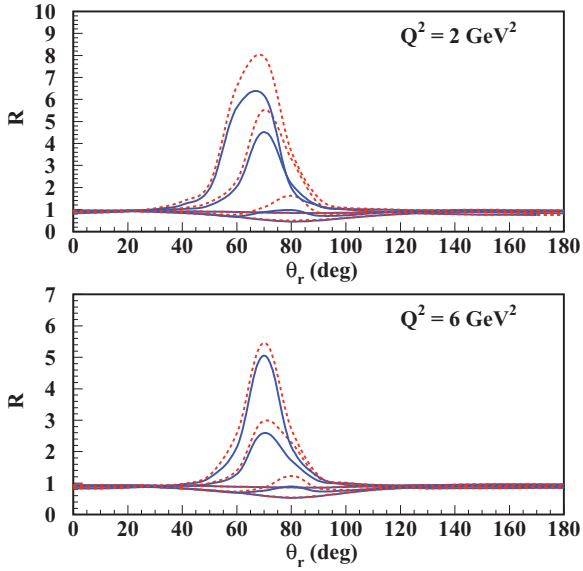

FIG. 5. (Color online) Dependence of ratio R on the recoil angle of the neutron for different values of p_r and $Q^2 = 2$, 6 GeV^2. The recoil neutron momenta are the same as in Fig. 3. Solid line, unfactorized approximation with the pole term only forward $pn \to pn$ rescattering; dashed line, unfactorized approximation including the pole terms for both forward $pn \to pn$ and charge-exchange $pn \to np$ rescattering amplitudes.

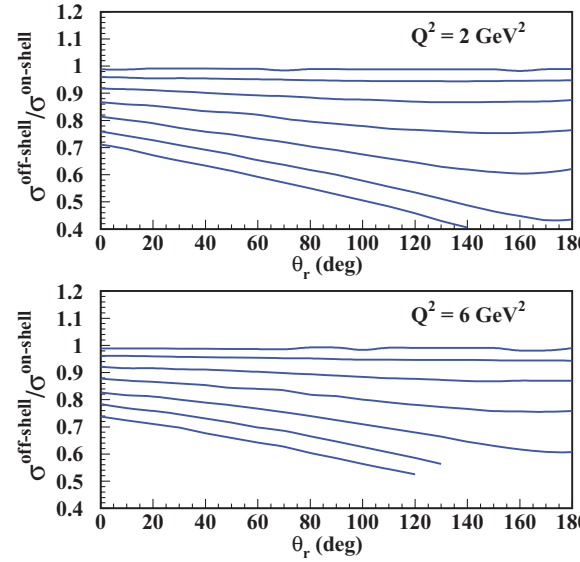

FIG. 6. (Color online) Ratio of PWIA cross sections calculated using on-shell and off-shell approximations for the electromagnetic current of the proton. The curves, from top to bottom, correspond to recoil neutron momenta of 100, 200, 300, 400, 500, 600, and 700 MeV/c, respectively.

the real part of the forward elastic FSI amplitude which is a small parameter at large energies. One can see from Fig. 5 that the charge-exchange rescattering dominates at kinematics in which the rescattering defines the overall magnitude of the cross section.

However, it is a rather well-known fact that, owing to the dominant pion-exchange nature of charge-exchange pn scattering, its cross section decreases linearly with an increase of the invariant energy s as compared to the forward pn elastic scattering cross section. As a result, one expects that with an increase of Q^2 the charge-exchange rescattering term will become a small correction. This can be seen from the calculation for $Q^2 = 6$ GeV^2 kinematics in Fig. 5.

D. Off-shell electromagnetic interaction effects

The preceding evaluations of the $d(e, e'p)n$ cross sections demonstrate that in the large Q^2 limit the property of the scattering is defined mainly by the PWIA and forward angle on-shell FSI terms. The angular distribution has a very characteristic shape in which one can identify kinematics dominated by PWIA or FSI. Calculations also show that the forward or backward kinematics of the recoil nucleon are best suited for isolating the PWIA term, which subsequently allows us to study the structure of the electromagnetic current of the bound nucleon and the deuteron wave function at large values of internal momenta.

We now concentrate on the effects related to the fact that the proton in the deuteron becomes increasingly off-shell at large values of recoil neutron momenta in forward or backward directions.

As follows from Eqs. (15), (18), and (20), the off-shell part of the electromagnetic current will diminish the overall magnitude of the electromagnetic interaction. Because the off-shellness grows with an increase of the initial momentum of the struck nucleon, it will result in the suppression of the electromagnetic interaction strength of deeply bound nucleons. As follows from Fig. 6, the off-shell effects have a weak Q^2 dependence and to disentangle them from the effects related to the high-momentum component of the deuteron wave function would require measurements covering an extended angular and recoil momentum range. Figure 6 also shows that the forward direction of recoil nucleon momenta represents the most optimal kinematic region for minimizing the off-shell effects for electromagnetic interaction.

Note that polarization measurements will provide additional observables for separating current and wave-function effects. For example, measurements of the cross section asymmetries similar to Ref. [65] at large recoil momenta will be more sensitive to the structure of the electromagnetic current because wave-function effects largely cancel out in the ratios defining the asymmetry.

E. Comparison with experimental data

In the past few years three experiments [25–27] produced first data at relatively large Q^2 kinematics.

The first experiment [25] probed the $Q^2 = 0.665$ GeV^2 and $x \approx 1$ kinematics and provided very accurate data. The measured value of Q^2 is marginal for the application of the GEA. However, as Fig. 7 shows, the comparison yields a surprisingly good agreement with the data. Figure 7 compares the reduced cross section defined as follows:

$$\sigma_{\rm red} = \frac{d\sigma}{dE'_e, d\Omega_{e'} dp_f d\Omega_f} \cdot \frac{\left|\frac{p_f}{E_f} + \frac{p_f - q\cos(\theta_{p_f,q})}{E_r}\right|}{\sigma_{\rm CC1} \cdot p_f^2}, \qquad (51)$$

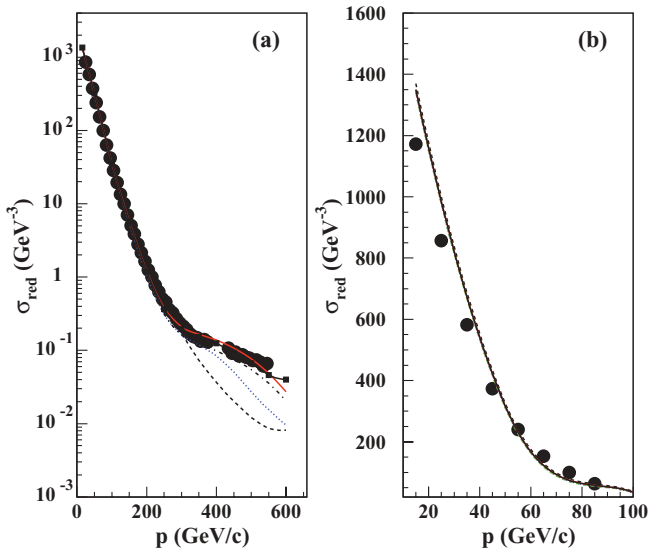

FIG. 7. (Color online) Missing momentum dependence of the reduced cross section. The data are from Ref. [25]. Dashed line, PWIA calculation; dotted line, PWIA + only pole term of forward FSI; dash-dotted line, PWIA + forward FSI; solid line, PWIA + forward and charge-exchange FSI; and solid line with squares, same as the previous solid line, plus the contribution from the mechanism in which the proton is a spectator and the neutron was struck by the virtual photon.

where the differential cross section is defined according to Eq. (46) and σ_{CC1} is the off-shell electron-proton cross section defined in Ref. [51]. Note that in this calculation for f_{pn} amplitude we use SAID [53] parametrization for both elastic and charge-exchange pn scatterings which fit the elastic pn scattering data for laboratory momenta up to 1.3 GeV/c. Because of the relatively low energy and momentum transfers involved in the reaction, the calculation shows a substantial contribution from the off-shell as well as charge-exchange parts of the FSI amplitude (difference between dotted, dash-dotted, and solid lines in Fig. 7). It is worth noting that our main goal is to calculate disintegration reaction in kinematics well above the region where SAID parametrization can be used. Thus, we are not pretending to improve further the calculation in the smaller $Q^2 \leqslant 1$ GeV^2 region and the present calculation is for illustration purposes only to ascertain how well eikonal approximation works for intermediate, $Q^2 \sim 1$ GeV^2, kinematics.

However, it is interesting that our calculation is in agreement with the observations of Refs. [27,38] that the theory overestimates the low-recoil-momentum part of the cross section [Fig. 7(b)], where we expect that theoretical uncertainties are well under the control. Our preliminary estimates demonstrate that this discrepancy could be accounted for by inclusion of the contribution of two-photon exchange effects in the overall amplitude of the scattering [66].

The second experiment [26] covered the Q^2 range from 2–5 GeV^2. However, owing to the low statistics, the data are integrated over the ranges of the recoil nucleon momenta.

Comparing with these data, we performed the same kinematic integrations as the experiment did. The results are shown

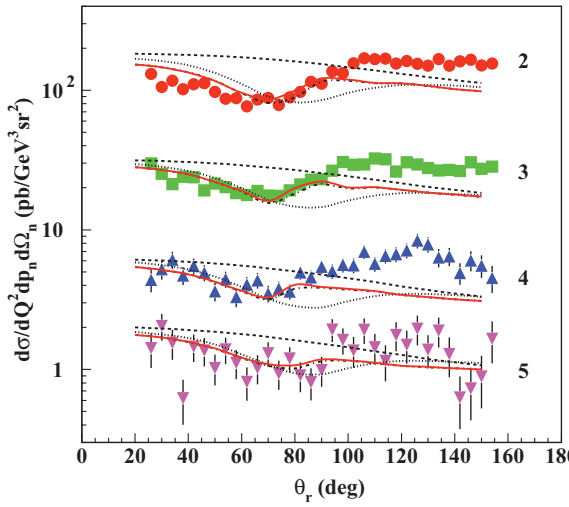

FIG. 8. (Color online) Dependence of the differential cross section on the direction of the recoil neutron momentum. The data are from Ref. [26]. Dashed line, PWIA calculation; dotted line, PWIA + pole term of forward FSI; dash-dotted line, PWIA + forward FSI; solid line, PWIA + forward and charge-exchange FSI. The momentum of the recoil neutron is restricted to $200 < p_r < 300$ MeV/c. The labels 2, 3, 4, and 5 correspond to the values of $Q^2 = 2 \pm 0.25$, 3 ± 0.5, 4 ± 0.5, and 5 ± 0.5 GeV^2.

in Figs. 8 and 9. Despite these integrations, we still can make several important observations from these comparisons.

(i) First, the angular distribution clearly exhibits an eikonal feature, with the minimum (Fig. 8) or maximum (Fig. 9) at transverse kinematics owing to the FSI. The most important result is that the maximum of FSI is at recoil angles of 70°, in agreement with the GEA prediction of Refs. [31,40]. A similar result was independently obtained also in Ref. [67]. Note that the conventional Glauber theory predicted 90° for the FSI maximum.

(ii) The disagreement of the calculation with the data at $\theta_r > 70°$ appears to be attributable to the isobar contribution at the intermediate state of the reaction.[4] This region corresponds to $x < 1$ and it is kinematically closer to the threshold of Δ-isobar electroproduction. The comparisons also indicate that the relative strength of the Δ-isobar contribution diminishes with an increase of Q^2 and at neutron production angles $\theta_r \to 180°$.

(iii) The forward direction of the recoil nucleon momentum, being far from the Δ-isobar threshold, exhibits a relatively small contribution owing to FSI. This indicates that the forward recoil angle region is best suited for studies of PWIA properties of the reaction such as the off-shell electromagnetic current and deuteron wave function.

Finally, the results of the experiment of Ref. [27] are currently in the final stages of analysis. Because in this

[4]The importance of the Δ-isobar contribution was pointed out earlier in Ref. [36].

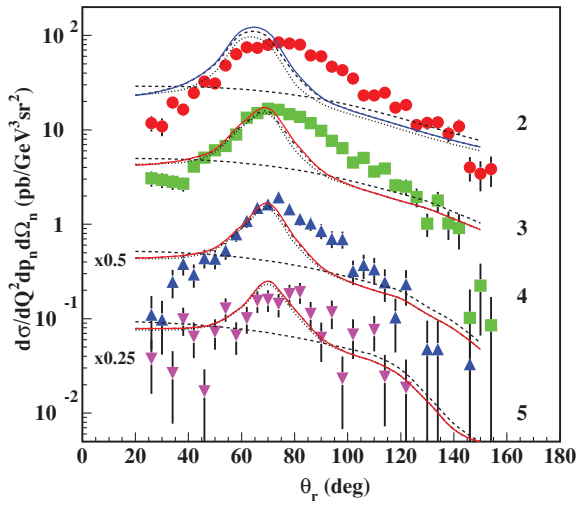

FIG. 9. (Color online) Dependence of the differential cross section on the direction of the recoil neutron momentum. The data are from Ref. [26]. Dashed line, PWIA calculation; dotted line, PWIA + pole term of forward FSI; dash-dotted line, PWIA + forward FSI; solid line, PWIA + forward and charge-exchange FSI. The momentum of the recoil neutron is restricted to $400 < p_r < 600$ MeV/c. The labels 2, 3, 4, and 5 correspond to the values of $Q^2 = 2 \pm 0.25$, 3 ± 0.5, 4 ± 0.5, and 5 ± 0.5 GeV^2, respectively. The data sets and calculations for 4 and 5 are multiplied by 0.5 and 0.25, respectively.

experiment the disintegration reaction is measured at forward recoil angles and at Q^2 up to 3.5 GeV^2, we expect that it will allow us to further check the validity of our claim that the forward angular region is best suited for studies of the PWIA properties of the reaction.

IV. CONCLUSIONS

Within the virtual nucleon approximation we developed a theoretical framework for calculation of high Q^2 exclusive electrodisintegration of the deuteron at large values of recoil nucleon momenta. The scattering amplitude is derived based on the GEA, in which case each amplitude is calculated based on effective Feynman diagram rules. Because of the covariant formulation of the problem, the electromagnetic current is gauge invariant from the beginning. By isolating the off-shell part in the electromagnetic current, we introduced an approach that allows us to express the bound nucleon current separately through the on-shell and of-shell parts.

Next, we derived the FSI amplitude based on the GEA and expressed it through the on-shell and off-shell rescattering parts. No factorization approximation is assumed in the calculation of the FSI amplitude. The calculation of FSI also includes the amplitude owing to the charge-exchange FSI.

We performed numerical analysis of the obtained formulas to identify the level of uncertainties owing to the factors included in the calculations. Overall, our conclusion is that with an increase of Q^2 all the uncertainties related to the off-shell FSI and charge-exchange rescattering became small and the total scattering amplitude is determined by the PWIA and on-shell elastic NN rescattering.

We compared our calculations with the first experimental data at large Q^2 deuteron electrodisintegration. These comparisons revealed a rather surprising agreement with low $Q^2 = 0.665$ GeV^2 data, which indicates the wider range of applicability of the present approximation.

Comparisons with higher Q^2 data ($\geqslant 2$ GeV^2) at the wider range of recoil nucleon momenta and angles demonstrate the important role that the intermediate Δ-isobar production plays in electrodisintegration reaction at backward angles close to the Δ production threshold.

However, at forward recoil angles where FSI effects are restricted, the calculations show greater sensitivity to the PWIA structure of the electrodisintegration reaction. Further experiments will allow us to confirm that this region is most suitable for probing the bound nucleon electromagnetic current and the deuteron wave function at small distances.

ACKNOWLEDGMENTS

I am thankful to Werner Boeglin, Mark Strikman, and late Kim Egiyan for numerous discussions on the physics of deuteron breakup. I regret that this work was completed too late for Kim to see the importance of his deuteron breakup experiment. This work is supported by the US Department of Energy Grant under Contract No. DE-FG02-01ER41172.

[1] V. G. J. Stoks, R. A. M. Klomp, C. P. F. Terheggen, and J. J. de Swart, Phys. Rev. C **49**, 2950 (1994).
[2] R. B. Wiringa, V. G. J. Stoks, and R. Schiavilla, Phys. Rev. C **51**, 38 (1995).
[3] R. Machleidt, Phys. Rev. C **63**, 024001 (2001).
[4] M. Lacombe, B. Loiseau, J. M. Richard, R. Vinh Mau, J. Conte, P. Pires, and R. de Tourreil, Phys. Rev. C **21**, 861 (1980).
[5] S. Sawada, Nucl. Phys. A **782**, 434 (2007).
[6] M. F. Lutz, B. Pire, O. Scholten, and R. Timmermans (PANDA Collaboration), arXiv:0903.3905 [hep-ex].
[7] L. L. Frankfurt and M. I. Strikman, Phys. Rep. **76**, 215 (1981).
[8] L. L. Frankfurt and M. I. Strikman, Phys. Rep. **160**, 235 (1988).
[9] M. M. Sargsian *et al.*, J. Phys. G **29**, R1 (2003).
[10] M. M. Sargsian, Int. J. Mod. Phys. E **10**, 405 (2001).
[11] L. Frankfurt, M. Sargsian, and M. Strikman, Int. J. Mod. Phys. A **23**, 2991 (2008).
[12] L. L. Frankfurt, M. I. Strikman, D. B. Day, and M. Sargsian, Phys. Rev. C **48**, 2451 (1993).
[13] K. S. Egiyan *et al.* (CLAS Collaboration), Phys. Rev. C **68**, 014313 (2003).
[14] K. S. Egiyan *et al.* (CLAS Collaboration), Phys. Rev. Lett. **96**, 082501 (2006).
[15] R. Shneor *et al.* (Jefferson Lab Hall A Collaboration), Phys. Rev. Lett. **99**, 072501 (2007).
[16] R. Subedi *et al.*, Science **320**, 1476 (2008).
[17] Y. Mardor *et al.*, Phys. Lett. B **437**, 257 (1998).
[18] J. L. S. Aclander *et al.*, Phys. Lett. B **453**, 211 (1999).
[19] A. Tang *et al.*, Phys. Rev. Lett. **90**, 042301 (2003).

[20] I. Yaron, L. Frankfurt, E. Piasetzky, M. Sargsian, and M. Strikman, Phys. Rev. C **66**, 024601 (2002).
[21] E. Piasetzky, M. Sargsian, L. Frankfurt, M. Strikman, and J. W. Watson, Phys. Rev. Lett. **97**, 162504 (2006).
[22] M. M. Sargsian, T. V. Abrahamyan, M. I. Strikman, and L. L. Frankfurt, Phys. Rev. C **71**, 044615 (2005).
[23] R. Schiavilla, R. B. Wiringa, S. C. Pieper, and J. Carlson, Phys. Rev. Lett. **98**, 132501 (2007).
[24] M. Alvioli, C. Ciofi degli Atti, and H. Morita, Phys. Rev. Lett. **100**, 162503 (2008).
[25] P. E. Ulmer *et al.*, Phys. Rev. Lett. **89**, 062301 (2002).
[26] K. S. Egiyan *et al.* (the CLAS Collaboration), Phys. Rev. Lett. **98**, 262502 (2007).
[27] W. U. Boeglin, Eur. Phys. J. A **24**, 77 (2005); L. Coman, Ph.D. thesis, Florida International University, Miami, 2008.
[28] *White Paper: The Science Driving the 12 GeV Upgrade of CEBAF* (Jefferson Lab, Newport News, VA, 2000).
[29] L. Frankfurt, E. Piasetsky, M. Sargsian, and M. Strikman, Phys. Rev. C **51**, 890 (1995).
[30] A. Bianconi, S. Jeschonnek, N. N. Nikolaev, and B. G. Zakharov, Phys. Lett. B **343**, 13 (1995).
[31] L. L. Frankfurt, W. R. Greenberg, G. A. Miller, M. M. Sargsian, and M. I. Strikman, Z. Phys. A **352**, 97 (1995).
[32] L. L. Frankfurt, E. Piasetzky, M. M. Sargsian, and M. I. Strikman, Phys. Rev. C **56**, 2752 (1997).
[33] S. Jeschonnek, Phys. Rev. C **63**, 034609 (2001).
[34] C. Ciofi degli Atti, L. P. Kaptari, and D. Treleani, Phys. Rev. C **63**, 044601 (2001).
[35] C. Ciofi degli Atti and L. P. Kaptari, arXiv:nucl-th/0407024.
[36] J. M. Laget, Phys. Lett. B **609**, 49 (2005).
[37] S. Jeschonnek and J. W. Van Orden, Phys. Rev. C **78**, 014007 (2008).
[38] S. Jeschonnek and J. W. Van Orden, Phys. Rev. C **80**, 054001 (2009).
[39] J. J. Adam, F. Gross, S. Jeschonnek, P. Ulmer, and J. W. Van Orden, Phys. Rev. C **66**, 044003 (2002).
[40] L. L. Frankfurt, M. M. Sargsian, and M. I. Strikman, Phys. Rev. C **56**, 1124 (1997).
[41] M. M. Sargsian, T. V. Abrahamyan, M. I. Strikman, and L. L. Frankfurt, Phys. Rev. C **71**, 044614 (2005).
[42] C. Ciofi delgi Atti and L. P. Kaptari, Phys. Rev. Lett. **100**, 122301 (2008).
[43] M. Alvioli, C. Ciofi degli Atti, and L. P. Kaptari, Phys. Rev. C **81**, 021001 (2010).
[44] M. M. Sargsian, S. Simula, and M. I. Strikman, Phys. Rev. C **66**, 024001 (2002).
[45] M. Sargsian and M. Strikman, Phys. Lett. B **639**, 223 (2006).
[46] P. Stoler, Phys. Rept. **226**, 103 (1993).
[47] M. Ungaro *et al.* (CLAS Collaboration), Phys. Rev. Lett. **97**, 112003 (2006).
[48] M. Sargsian (unpublished).
[49] V. N. Gribov, Sov. Phys. JETP **30**, 709 (1970).
[50] L. Bertuchi, Nuovo Cimento A **11**, 45 (1972).
[51] L. De Forest, Nucl. Phys. A **392**, 232 (1983).
[52] G. P. Lepage and S. J. Brodsky, Phys. Rev. D **22**, 2157 (1980).
[53] R. A. Arndt, W. J. Briscoe, I. I. Strakovsky, and R. L. Workman, Phys. Rev. C **76**, 025209 (2007).
[54] J. Bystricky, F. Lehar, and P. Winternitz, J. Phys. **39**, 1 (1978).
[55] W. R. Gibbs and B. Loiseau, Phys. Rev. C **50**, 2742 (1994).
[56] R. A. Gilman and F. Gross, J. Phys. G **28**, R37 (2002).
[57] L. L. Frankfurt and M. I. Strikman, Phys. Lett. B **64**, 433 (1976); **183**, 254 (1987).
[58] P. V. Landshoff and J. C. Polkinghorne, Phys. Rev. D **18**, 153 (1978).
[59] M. M. Sargsian, L. L. Frankfurt, and M. I. Strikman, Z. Phys. A **335**, 431 (1990).
[60] C. Ciofi degli Atti and S. Liuti, Phys. Rev. C **41**, 1100 (1990).
[61] L. L. Frankfurt, G. A. Miller, M. M. Sargsian, and M. I. Strikman, Phys. Rev. Lett. **84**, 3045 (2000).
[62] J. J. Kelly, Phys. Rev. C **70**, 068202 (2004).
[63] L. L. Frankfurt, W. R. Greenberg, G. A. Miller, M. M. Sargsian, and M. I. Strikman, Phys. Lett. B **369**, 201 (1996).
[64] K. Egiian, L. Frankfurt, W. R. Greenberg, G. A. Miller, M. Sargsian, and M. Strikman, Nucl. Phys. A **580**, 365 (1994).
[65] S. Strauch *et al.* (Jefferson Lab E93-049 Collaboration), Phys. Rev. Lett. **91**, 052301 (2003).
[66] M. Sargsian (unpublished).
[67] J. M. Laget, *Proceedings of the Workshop on Color Transparency, Grenoble, France, 25–27 June 1997*, edited by E. Voutier (Institute de Sciences Nucleaires, Grenoble, 1998), p. 121.